Solid-State NMR and Small-Angle X-ray Scattering Study of Microphase Structure of Amorphous and Semicrystalline Poly(styrene−ethylene oxide) Diblock Copolymers

Hongshi Yu,[†] Almeria Natansohn,*[,†] Marsha A. Singh,[‡] and Iris Torriani[§]

Department of Chemistry, Queen's University, Kingston, Ontario, Canada K7L 3N6; Department of Physics, Queen's University, Kingston, Ontario, Canada K7L 3N6; and National Synchrotron Light Laboratory (LNLS)/CNPq, Campinas, SP, Brazil

Received June 27, 2000

ABSTRACT: The microphase structure of a series of poly(styrene−ethylene oxide) (SEO) block copolymers has been studied by solid-state NMR and small-angle X-ray scattering (SAXS) techniques. The differential scanning calorimetry studies indicate that the majority of SEO samples are semicrystalline. For the completely amorphous SEO, solid-state NMR ^{1}H spin diffusion was used to determine the sizes of various domains, interfacial thickness, and interdomain distances by the initial-rate approximation and by numerical simulation with a pure spin diffusion model. The results obtained from the above two methods, the initial-rate approximation and the numerical simulation, are generally in good agreement, but the interdomain distance estimated from NMR is relatively lower than that obtained from SAXS. The discrepancy is probably caused by the simulation model used in the NMR data interpretation. For the semicrystalline SEO samples, the relative locations of multiple Bragg peaks and the location of the first-order maximum in the SAXS data were used to determine the morphology and the size of the interdomain distance of the material. This is a typical example where either NMR or SAXS alone cannot yield complete phase structure information for both amorphous and semicrystalline SEO materials. A combination of the above two techniques is necessary and allows us to explore the phase structure of both the amorphous and the semicrystalline SEO samples and also examine the validity of the pure spin diffusion model used for the NMR analysis.

1. Introduction

A common characteristic of multicomponent block copolymers in the solid state is their ability to exhibit microphase-separated structures. The formation of microdomains and their phase structures are generally responsible for many novel and useful properties of block copolymers, such as processability and thermal, mechanical, optical, and transport properties.[1] There are generally two classes of block copolymer systems in terms of their chain architecture: one is the system with two completely amorphous blocks; the other one is the system in which one block can crystallize. It has been established, especially by transmission electron microscopy (TEM), scanning electron microscopy (SEM), and small-angle X-ray scattering (SAXS), that the microdomain structure can be spheres, cylinders, and lamellae. Helfand has extensively studied the microdomain structure of polystyrene−polybutadiene diblock copolymers and found that the type of morphology adopted by the copolymer generally depends on the chemical composition of the two blocks and that the total molecular weight of the copolymer has much less importance.[2]

Block copolymers with one component semicrystalline and the other amorphous are particularly interesting materials in terms of their crystal structure, morphology, crystallization kinetics, and dynamics. The reason is that the covalent bonding of the two chemically dissimilar blocks, composed of amorphous and crystalline segments, produces a new material whose properties are not simple functions of the individual homopolymers. Among these systems, poly(styrene−ethylene oxide) (SEO) diblock copolymers have been studied extensively, mainly because of the great block dissimilarity and incompatibility. Earlier studies by Gervais and Gallot[3−5] have found that a lamellar crystalline structure was formed below 50 °C for SEO materials in the dry state and in a preferential solvent for PEO. In these lamellar structures, the elementary sheet is formed by the superposition of the two layers. The first contains the amorphous blocks; the second contains the crystallized and refolded chains.[3−5] Unlike crystallizable homopolymers, where the chain folding is metastable, folding of the partly crystallizable blocks of copolymers exists at equilibrium, in which case it is governed by a balance of the thermodynamic forces between the crystalline and the amorphous domains.[6] Recently, Floudas et al.[7] have studied the crystallization kinetics of PEO in poly(ethylene oxide−styrene-ethylene) triblock copolymers, and their results are in favor of a multilayer lamellar morphology of PEO with a spherulitic superstructure. However, very little is known about the interfacial structure between the crystalline PEO and the amorphous PEO and the interfacial structure between the amorphous polystyrene and amorphous PEO.

Various experimental techniques, such as differential scanning calorimetry (DSC), scanning electron microscopy, transmission electron microscopy, small-angle X-ray scattering, and solid-state NMR techniques, can be used to investigate the phase structure of both amorphous and semicrystalline materials. Spin−lattice relaxation times in the laboratory [T_1(H)] and in the rotating frame [$T_{1\rho}$(H)] are sensitive to heterogeneity

* Author to whom correspondence should be addressed.
† Department of Chemistry, Queen's University.
‡ Department of Physics, Queen's University.
§ National Synchrotron Light Laboratory (LNLS)/CNPq.

10.1021/ma001127b CCC: $20.00
Published on Web 01/24/2001

in the materials. The latter has been used as a convenient probe to identify the separated minority phase at a level of a few nanometers. Interfacial structure is very important to the use properties of polymer materials, and normally it is not easy to access due to the limited resolution of the majority of applicable probes. Solid-state NMR techniques offer the possibility of high-resolution measurements of the interface. Measurements of proton spin diffusion by solid-state NMR have been proven to be very powerful in investigating phase structures of multicomponent materials, such as polymer blends,[8−10] block copolymers,[11−15] and semicrystalline polymer materials.[16−19] The experiment contains three steps: an initial pulse destroys the magnetization of one component and leaves the magnetization of the other component as a magnetization source. In the following mixing time, the magnetization can redistribute in space by "spin diffusion". The distribution of the magnetization in the material is then detected for varying mixing time. The phase structure parameters of the materials can be extracted through computer simulation of the NMR signal intensities as a function of mixing time in the spin diffusion process. A few models have been developed and used to obtain the domain size and interfacial thickness from solid-state NMR measurements.[20−22] Our previous studies indicated that the spin diffusion curves are well reproduced by a model that considers the T_1 effects for all the studied materials, and its results are in better agreement with the SAXS results than those obtained using the pure spin diffusion model.[23,24]

SAXS is a very powerful method to study the phase separation process and determine microdomain sizes, but the absence of strong electron density contrasts between the components in some materials is a potential obstacle for using this technique. Solid-state NMR provides an alternative method to study the microphase structure of these samples. As mentioned previously, solid-state NMR measurements of ^{1}H spin diffusion have been successfully used to investigate the phase structure in many polymer materials[8−19] However, in the case of semicrystalline polymer materials, most of the studies are limited to semicrystalline homopolymers. Generally speaking, it is difficult to apply known solid-state NMR spin diffusion techniques to obtain a spin diffusion curve for semicrystalline block copolymers due to their very complicated phase structure, while SAXS is generally very efficient in exploring phase structure given the electron density contrast between amorphous and crystalline phases. The combination of solid-state NMR and SAXS is therefore an ideal choice to investigate these materials.

In this paper, the phase structure of both amorphous and semicrystalline poly(styrene−ethylene oxide) block copolymers, especially the interfacial structure between the crystalline PEO and amorphous PEO and the interfacial structure between the amorphous polystyrene and PEO, was investigated using solid-state NMR and SAXS techniques. This is a typical example where the two techniques, NMR and SAXS, are complementary for the determination of the microphase structure of polymer materials.

2. Experimental Section

2.1. Samples. Poly(styrene−ethylene oxide) (SEO) diblock copolymers and poly(ethylene oxide) (PEO) homopolymer were purchased from Polymer Source, Inc., and the chemical structure of SEO is shown in Scheme 1. The weight ratios of

Scheme 1

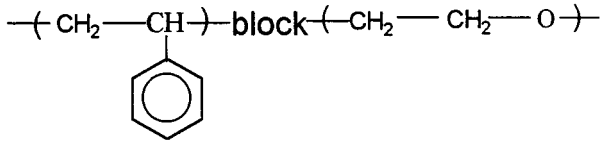

Polystyrene (PS) Poly(ethylene oxide) (PEO)

Table 1. Characterization of SEO and PEO Samples

sample code	wt ratio (PS/PEO)	vol fraction of PS	total M_n (kg/mol)	M_n of S block (kg/mol)	M_w/M_n
SEO-1	66/34	0.68	97.2	64	1.06
SEO-2	43/57	0.45	9.0	3.9	1.06
SEO-3	12/88	0.13	53.0	6.1	1.08
SEO-4	34/66	0.36	36.1	12.2	1.05
SEO-5	31/69	0.33	52.8	16.4	1.06
PEO			34.1	1.13	

the polystyrene and poly(ethylene oxide) in SEO samples taken from the characterization data provided by Polymer Source, Inc., and the volume fractions obtained from the weight ratios using the known densities of polystyrene[25] and poly(ethylene oxide)[26] ($\rho_{PS} = 1.05$ g/cm^3; $\rho_{PEO} = 1.13$ g/cm^3) are given in Table 1. Solution NMR was used to confirm these values, and results are generally in very good agreement. In the following section, the abbreviation SEO-n (n = 1, 2, ..., 5) will be used for the five samples. The molecular weights and polydispersities of these samples are also given in Table 1.

2.2. Sample Preparation. For the amorphous SEO sample, films were prepared and used for both NMR and SAXS measurements in order to compare the results from the two techniques. The film specimens were obtained from a THF solution of 5 wt % polymer concentration by slowly evaporating the solvent at room temperature for 4 days. To further remove the THF, the films were vacuum-dried at room temperature for about 3 days. For the NMR measurements, samples were prepared by cutting the film into 2−3 mm^2 pieces.

For semicrystalline SEO samples, the film was obtained by annealing the samples in a heated compression-mold at 120 °C for 20 min and then rapidly quenching to room temperature.

2.3. NMR Measurements. All solid-state NMR measurements were performed on a Bruker ASX-200 spectrometer operating at 200 and 50.29 MHz for ^{1}H and ^{13}C, respectively. The rotors were spun at about 5.0 kHz in order to avoid overlapping of spinning sidebands and other peaks. The $\pi/2$ pulse is about 4.2 μs with an optimum contact time of 1.5 ms. The carbon detection was achieved through cross-polarization (CP), magic angle spinning (MAS), and dipolar decoupling (DD), and all spectra were obtained at room temperature.

^{1}H spin diffusion measurements were performed using a dipolar filter pulse sequence.[27] The selection of the magnetization of the mobile PEO component was achieved by repeating cycles with a delay time of 11 μs for five times. Phase cycling (PC, an alternating of a π pulse and no pulse) was used after the selection to eliminate the T_1 spin−lattice relaxation effects in the spin diffusion process. ^{1}H T_1 spin−lattice relaxation times were measured using an inversion−recovery pulse sequence through cross-polarization to ^{13}C.

2.4. SAXS Measurements. Small-angle X-ray scattering measurements were performed at the SAXS beamline[28] of the Laboratorio Nacional de Luz Síncrotron (LNLS) in Campinas, Brazil. All of the measurements were made using a Kodak SO-230 image plate with a spatial resolution of 218 μm at a wavelength of 1.608 Å (6.9 keV) and sample-to-detector distance of 1256.5 mm. The minimum accessible angle, as seen in the analysis plots, is about 0.07 Å^{-1}.

The image plate is a 2-dimensional detector. Preliminary 2-D scattering profile are reduced to 1-D data using the program X-RAY, version 1.0 (1996), Université Mons Hainaut, for further background correction and analysis.

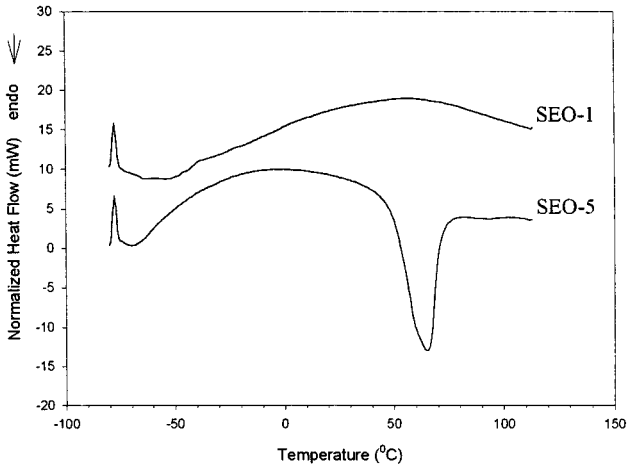

Figure 1. DSC curves of different SEO samples (heating rate: 20 K/min).

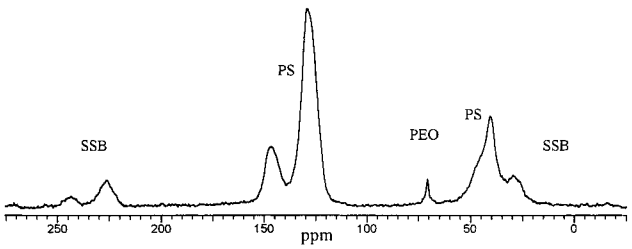

Figure 2. CP/MAS ^{13}C spectrum of SEO-1 sample.

3. Results and Discussion

3.1. Thermal Analysis. DSC measurements were performed for all six samples over the temperature range −80 to 170 °C with a heating rate of 20 °C/min, and typical plots in the form of heat flow as a function of temperature for the SEO-1 and the SEO-5 samples are shown in Figure 1.

It can be seen from Figure 1 that a weak transition for the SEO-1 sample occurs at a temperature of about −30 °C. This is in accordance with the glass transition temperature of bulk PEO homopolymers reported in the literature.[26] The bulk PEO is a semicrystalline polymer with a glass transition $T_g = -41$ °C and a melting temperature $T_m = 67$ °C. The glass transition temperature[26] of polystyrene is about 100 °C, but this is not seen with the SEO-1 sample. For all other SEO and PEO samples, no PS and PEO glass transitions were seen, but a very strong endothermic peak corresponding to the melting point at about 67 °C was found for SEO-2, SEO-3, SEO-4, SEO-5, and PEO samples, indicating that all of these samples are semicrystalline. Only SEO-1, where the crystallizable PEO block is a minor component, is completely amorphous, whereas all other SEO samples, although of different molecular weights and chemical compositions, are semicrystalline.

3.2. Spin Diffusion in the Amorphous SEO Sample. Solid-state NMR measurements of ^1H spin diffusion were used to explore the microphase structure of the amorphous SEO-1 sample. Figure 2 shows a CP/MAS ^{13}C spectrum of the SEO-1 sample, and the assignment of each peak is straightforward. The peaks at about 127 and 146 ppm come from the protonated and nonprotonated aromatic carbons of the PS, respectively, while the peak at about 71 ppm is attributed to the amorphous PEO. SSB are spinning sidebands. For each resolved signal, $T_1(H)$ values were measured, and the results are given in Table 2. The intrinsic $T_1(H)$'s

Table 2. $T_1(H)$ Values for the Amorphous SEO-1, PS, and PEO Samples

sample code	$T_1(H)$ for the PS block (ms)	$T_1(H)$ for the PEO block (ms)
SEO-1	779 ± 50	594 ± 30
PS	1600 ± 100	
PEO		1200 ± 105

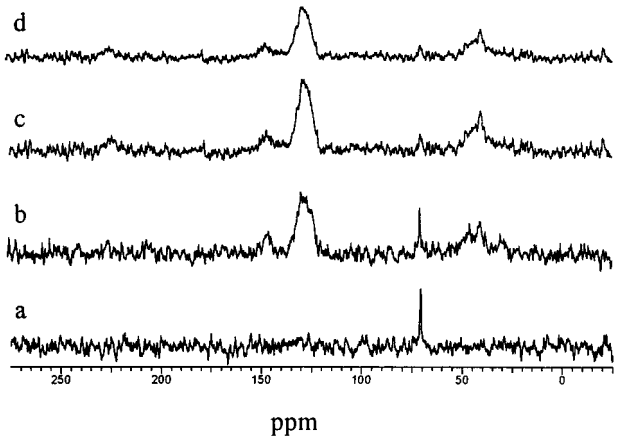

Figure 3. Dipolar filter spectra of SEO-1 at different mixing times: (a) 750 μs, (b) 40 ms, (c) 200 ms, and (d) 600 ms.

of the two components in the SEO-1 sample are the corresponding homopolymer values: 1600 ms for PS and 1200 ms for PEO. However, the $T_1(H)$ of the semicrystalline PEO homopolymer cannot be used as the intrinsic $T_1(H)$ of the amorphous ethylene oxide block, since the value of 1200 ms is an average for the crystalline and amorphous phases. The crystallization rate of pure PEO is too rapid to achieve a purely amorphous system by liquid nitrogen quenching. Therefore, it was not possible to obtain an intrinsic $T_1(H)$ for amorphous PEO.

3.2.1. Dipolar Filter Experiment. The mobility difference between the PS and amorphous PEO phases of SEO allows us to apply the dipolar filter pulse sequence to select the magnetization of the mobile PEO component. The dipolar filter pulse sequence used in this work has been described previously,[23] it consists of 12 $\pi/2$ pulses separated by a delay time, and the cycle can be repeated several times. During the mixing time, the protons in the rigid polystyrene component gain magnetization from the protons in the mobile PEO component through spin diffusion with the final spectra recorded through carbon detection. In Figure 3, a series of carbon spectra at different mixing times for the SEO-1 sample in the dipolar filter experiment are shown.

It can be seen from Figure 3 that only the signal from mobile PEO was selected, and the magnetization of the rigid polystyrene was removed by the filter at very short mixing times. With increasing mixing times, signals from the polystyrene appear, and their intensities increase while the signal intensity of PEO decreases. As previously discussed in the literature,[14,20] the signal intensity from spin−lattice relaxation (T_1) cannot be distinguished from the spin diffusion, and the T_1 effects can be reduced by switching the signal to $+z$ and $-z$ axes in alternating scans through a phase cycling pulse. However, the phase cycling also gives rise to a reduction in the overall intensity of the magnetization measured, and the form of this reduction is given by $\exp(t_m/T_1)$, where t_m is the mixing time and T_1 is the spin−lattice relaxation time in the laboratory frame for the resonance being measured. The intensities of the protonated

Table 3. ^{1}H Spin Diffusion Coefficients D_{PB} and ^{1}H NMR Line Widths $\Delta\nu_{1/2}$ of Polybutadiene at Different Temperatures[31]

T (K)	D_{PB} (nm^2/ms)	$\Delta\nu_{1/2}$ (Hz)
283	0.06 ± 0.015	560 ± 100
297	0.05 ± 0.015	150 ± 50
343	0.02 ± 0.010	70 ± 25

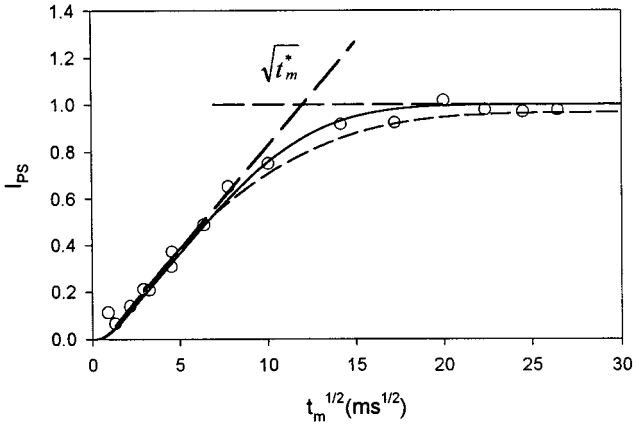

Figure 4. Magnetization growth of the protonated aromatic carbon signal as a function of mixing time (circles). The solid line is the fitting curve using the pure spin diffusion model with $\epsilon = 1$ (lamellar structure). The dashed line is the fitting curve using the pure spin diffusion model with $\epsilon = 2$ (cylindrical structure). The relatively long-dashed straight lines are used for the initial-rate approximation.

PS signal at different mixing times were corrected by multiplying by this factor, and a T_1 value of 779 ms, as listed in Table 3 for SEO-1, was used to correct the intensity of the PS signal in Figure 3. The results are shown in Figure 4 as circles.

3.2.2. Determination of the Spin Diffusion Coefficient of Amorphous PEO. In analyzing spin diffusion curves, values for the spin diffusion coefficients of both the PS and the PEO phases are required. Estimation of the spin diffusion coefficient can be done from the ^{1}H line shape.[20] However, PEO is semicrystalline, and calculation of the spin diffusion coefficient is difficult since the ^{1}H line is neither purely Gaussian nor Lorentzian. Instead, it contains a narrow amorphous component, superimposed on a broad line due to the crystalline structure.[29]

One solution is to calibrate the spin diffusion coefficient by fitting the spin diffusion data with parameters from a known domain structure.[14,20] Recently, Wilhelm et al. have discussed the spin diffusion coefficient of PEO, and a value of 0.1 nm^2/ms at 253 K was determined by simulating the spin diffusion curve with a set of domain size parameters obtained from SAXS.[30] This value is much lower than the value for PS reported in the literature,[20] $D_{PS} = 0.8$ nm^2/ms, but higher than the highly mobile polybutadiene[31] at 297 K, $D_{PB} = 0.05$ nm^2/ms. Since the spin diffusion coefficient is approximately proportional to the ^{1}H line width at half-height, it is an indication of polymer mobility at the measuring temperature, and the value will depend on temperature. Spiegel et al.[31] have studied the relationship between the temperature, ^{1}H line width, and the spin diffusion coefficient for poly(styrene−butadiene) diblock copolymers, and the results are listed in Table 3 for comparison.

From Table 3, it can be seen that, with every 10 K increase in temperature, the spin diffusion coefficient of polybutadiene is approximately reduced by 0.01 nm^2/ms. This observation was used as a general guide to estimate the spin diffusion coefficient of PEO at room temperature (293 K). A value of 0.07 ± 0.01 nm^2/ms is taken as a good estimate for PEO at 293 K, and this value is in reasonable agreement with the value obtained by Mellinger et al.[32] using T_2 measurements. Recently, Mellinger et al.[32] have discussed the possibility of calibrating the spin diffusion coefficient through the transverse relaxation rate T_2^{-1}, and different regimes were observed for T_2^{-1} below and above 1 kHz. A value of about 0.02 nm/ms^2 spin diffusion coefficient for the amorphous PEO phase at 373 K was estimated from their measurements. Within this context, the estimated value of 0.07 nm/ms^2 seems very reasonable.

It should be noted that the determination of the spin diffusion coefficient for mobile phases is more complex as it is particularly sensitive to different motions, including the sample spinning, and thus is dependent on the particular experimental conditions. Our estimation is based on the assumption that the spin diffusion coefficient does not change significantly at slightly different rotor speeds. However, there are always some uncertainties.

3.2.3. Initial-Rate Approximation and Numerical Simulation. As discussed by Clauss et al.,[20] the evaluation of the spin diffusion equation can be done by initial-rate approximation or by numerical simulation. For systems in which the interfacial thickness is small with respect to the size of domains, the average of the dispersed phase can be obtained using the initial-rate approximation, and the equation is given in the following,[20]

$$d_{dis} = \frac{\rho_A^H \Phi_A + \rho_B^H \Phi_B}{\Phi_A \Phi_A} \frac{\sqrt{D_A D_B}}{\sqrt{D_A}\rho_H^A + \sqrt{D_B}\rho_B^H} \frac{4\epsilon\Phi_{dis}}{\sqrt{\pi}} \sqrt{t^*_m} \quad (1)$$

where ρ^H, Φ, and D are the proton densities, volume fractions, and spin diffusion coefficients, respectively, for the two components A and B. ϵ is the dimensionality, and d_{dis} is the average size of the dispersed phase. It can be seen from this equation that, for a given spin diffusion curve, the estimated domain sizes will depend on the dimensionality. It has been found that the morphology of block copolymers is mainly dependent on the volume fraction of the dispersed phase. However, it is difficult to definitely determine the morphology of the SEO-1 sample since the composition of this sample as given in Table 1 is in the range of cylinders to lamellae phase structure transitions.[2] We assume that either a lamellar ($\epsilon = 1$) or cylindrical ($\epsilon = 2$) structure is formed for this sample on the basis of previous work.[2] $\sqrt{t^*_m}$ is determined by extrapolating the initial linear portion of the spin diffusion curve, and a value of 11.5 ms$^{1/2}$ is found for SEO-1, as shown in Figure 4. The long period, d_L (interdomain distance), and the size of the matrix, d_{mat}, can be obtained from the following relationships,[20]

$$d_L = d_{dis}/\sqrt[\epsilon]{\phi_{dis}} \quad (2)$$

$$d_L = d_{dis} + d_{mat} \quad (3)$$

The parameters used in the calculation and the results obtained by this method for SEO-1 are given in Table 4. The uncertainty in the domain sizes is estimated from two possible sources: one may be introduced

Table 4. Some Parameters and the Domain Size Results Obtained from Initial-Rate Approximation for SEO-1 Sample[a]

phase	proton density ρ^H (g/cm^3)	vol fraction ϕ	diffusion coeff D (nm^2/ms)	domain size ($\epsilon = 1$) (± 2 nm)	domain size ($\epsilon = 2$) (± 2 nm)
PS	0.081	0.68	0.80	$d_{mat} = 17$	$d_{mat} = 12$
PEO	0.103	0.32	0.07	$d_{dis} = 8$	$d_{dis} = 16$

[a] $d_L = d_{PEO} + d_{PS} = 8 + 17 = 25$ nm for $\epsilon = 1$ (lamellar structure); 28 nm for $\epsilon = 2$ (cylindrical structure). d_L is the distance between PEO domains.

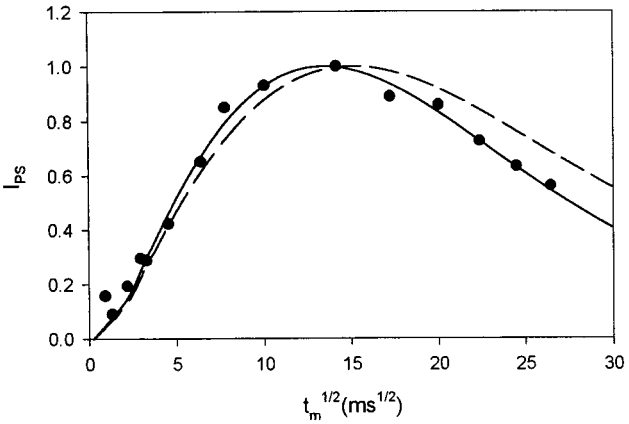

Figure 5. Magnetization growth of protonated aromatic carbons [without multiplying by a factor of $\exp(t_m/T_1)$] as a function of mixing times for SEO-1 sample (solid dots). The solid line is the fitting curve using the model which includes the T_1(H) term with the sizes of the PEO domain, $d_{PEO} = 16$ nm, interface, $d_I = 2$ nm, long period, $d_L = 32$ nm, and the hypothetical intrinsic T_1(H) for PEO of 300 ms. The dashed line is the fitting curve using the same model with the same domain sizes parameters but a different hypothetical intrinsic T_1(H) of 500 ms.

by the choice of spin diffusion coefficients; the other may be caused by the determination of the $\sqrt{t^*_m}$ parameter.

To more accurately extract the domain size information, a numerical simulation is needed. There are generally two kinds of models used in interpreting the spin diffusion process. One is the simulation model considering both the spin diffusion and the spin−lattice relaxation processes.[21] The other is the model considering only the spin diffusion process.[22] Both models have been described in detail by Wang et al.[21,22] It has been found that the domain size information obtained using a simulation model which includes T_1 spin−lattice relaxation term is more accurate than that obtained using a pure spin diffusion model.[23,24] However, in this case, the main limitation of this model is the dependence of the domain size parameters on the intrinsic T_1(H) of amorphous PEO. To further illustrate how important this value is, the spin diffusion curve for SEO-1 is simulated using the model including the T_1(H) effects. As the T_1(H) of the amorphous PEO in the copolymer is 594 ms (given in Table 2), the intrinsic T_1(H) must be lower because of the averaging effect in the copolymer. Two simulations with the same domain size parameters (the PEO domain size $d_{PEO} = 16$ nm, interface $d_I = 2$ nm, and long period $d_L = 32$ nm) but different hypothetical intrinsic T_1(H) values of the amorphous PEO are shown in Figure 5.

It can be seen that the two simulation curves are very different, especially in the later portion of the spin diffusion curve. This indicates that, without accurate intrinsic T_1(H) values for both components in the material, it is possible to introduce a relatively large error to the findings by simulating the spin diffusion curve with the model which includes T_1(H) effects. In this case, a pure spin diffusion model may be a better choice.

The spin diffusion process without considering the T_1 spin−lattice relaxation term can be described by the following diffusion equation:

$$\frac{\partial^2 c^A}{\partial x^2} - \frac{1}{D_A}\frac{\partial c^A}{\partial t_m} = 0 \qquad (4)$$

where c^A is the specific spin magnetization in component A and D_A is the spin diffusion coefficient of the A component; t_m is the diffusion time (mixing time). A similar equation exists for the B phase. To analyze the time dependence of the distribution of z-magnetization in a proton spin diffusion experiment, one generally has to solve the above diffusion equations. The equation should be solved with proper initial and boundary conditions, which contains domain size terms, as outlined by Wang.[22] The total spin magnetization in each phase, which is proportional to the NMR signal intensity, can be conveniently obtained by integrating the specific spin magnetization over the corresponding region, Ω_A or Ω_B, i.e.,

$$M^A(t) = \rho_H^A \int_{\Omega_A} c^A(r,t)\, dr \qquad (5)$$

where ρ_H^A is the proton concentration in the phase A. Simulated spin diffusion curves were obtained by plotting the total spin magnetization in the PS domains as a function of $\sqrt{t^*_m}$.

A system with a finite interface can be divided into three regions: source, sink, and interface. It is generally accepted that the chemical composition gradually changes across the phase boundaries, and this can be translated into a linear, sigmoidal, or trapezoidal change of the spin diffusion coefficient, proton density, as well as T_1 relaxation rate. For our pure spin diffusion model, we assume that linear changes of the spin diffusion coefficient and proton concentration occur across the interfacial region. This is the simplest and most often used assumption in the literature.

Simulations with the pure spin diffusion model for a one-dimensional lamellar and a two-dimensional cylindrical structure were carried out for the SEO-1 sample, and the best fits for each structure are shown in Figure 4 as a solid line and a dashed line, respectively. The best fitting parameters for the lamellar structure are the PEO domain size, $d_{PEO} = 8$ nm, interface, $d_I = 1.5$ nm, and long period $d_L = 29$ nm while for the cylindrical structure, they are the PEO domain $d_{PEO} = 14$ nm, interface, $d_I = 1.5$ nm, and interdomain distance $d_L = 27$ nm. These results are generally in good agreement with those obtained from the initial-rate approximation, respectively, indicating that the initial-rate approximation is reasonably effective for a sample with a relatively small interface.

It has been discussed in previous work[23,24] that, in general, the spin diffusion experiment cannot directly

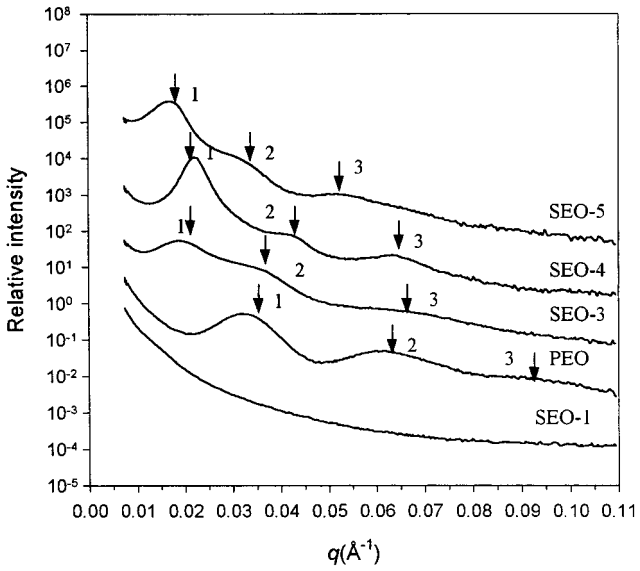

Figure 6. Synchrotron SAXS scattering intensity distribution after Lorentz correction in the Iq^2 as a function of scattering angle for the SEO and PEO samples.

provide morphological information. However, one may infer some morphological information by analyzing the linear behavior of the spin diffusion curve. Clauss et al.[20] have discussed the relationship between the linear behavior of the spin diffusion curve and the morphology and found that significant deviations from the linear behavior occur for structures with higher dimensionalities far earlier in the spin diffusion process than for structures with a low dimensionality. This effect can be used to determine the dimensionality of the phase structure in an investigated sample if sufficient quality data are available. It can be seen from Figure 4 that the deviations from the linear behavior for the simulation curve obtained from the two-dimensional cylindrical structure appear a little earlier than the experimental curve, while the fit is better for the simulation curve obtained from one-dimensional lamellar structure. Thus, tentatively, one may assume that a lamellar morphology is more likely for this sample.

3.3. SAXS Studies. To analyze the phase structure, especially interfacial structure, of semicrystalline SEO samples and to compare the results for the amorphous SEO-1 sample obtained from NMR, synchrotron SAXS studies were performed for all the SEO and PEO samples except for the SEO-2 due to an insufficient quantity of this sample.

3.3.1. Amorphous SEO-1 Sample. The synchrotron SAXS scattering pattern for the SEO-1 is shown in Figure 6, and no scattering peaks were found from this data profile. From Table 1, it can be seen that the SEO-1 sample has a relatively narrow polydispersity, and a long-range ordering scattering profile in the form of multiple Bragg peaks would normally be expected. This observed absence of structure could be explained by a very weak electron density contrast between the PS phase and the amorphous PEO phase. To enhance the peak structure in the SEO-1 sample, a plot in the form of Iq^4 vs q was carried out[33] and is shown in Figure 7 where a single weak, but definable, peak was found at $q = 0.015$ Å^{-1}.

A plane spacing, a, associated with the observable Bragg peak, can be calculated using an equation, $a = 2\pi/q_{max}$, and its value is about 42 nm. It has been

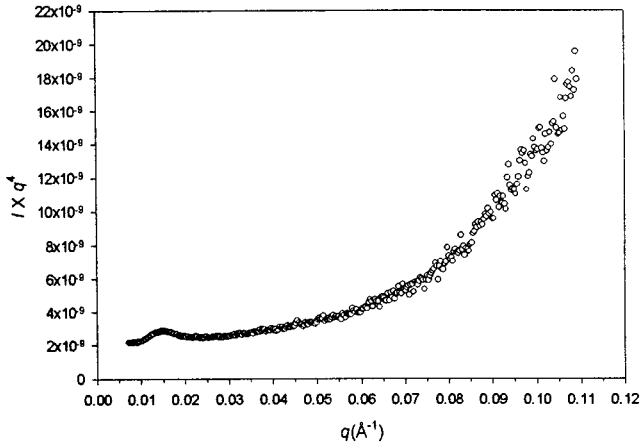

Figure 7. Synchrotron SAXS scattering plot in the form of Iq^4 as a function of q for the SEO-1 sample.

discussed by Sakurai et al.[34] that, for a well-ordered system with multiple diffraction peaks, different packing lattices will have different interdomain distances. The interdomain distances are given by a for simple cubic and lamellar structures, $1.15a$ for cylindrical structures, and $1.22a$ for body-centered-cubic and face-centered-cubic structures.[34] Therefore, the interdomain distance for the SEO-1 sample will be 42 nm for a lamellar structure and 48 nm for a cylindrical structure. It is then reasonable to assume that the effective interdomain distance of the sample lies in the range of 42−48 nm. The microphase structure results obtained from both NMR and SAXS are summarized in Table 5. It can be seen that the interdomain distance obtained from SAXS is consistently larger than the result obtained from the NMR method. The discrepancy between the NMR and SAXS results can probably be attributed to the pure spin diffusion model used in the spin diffusion data analysis.[24]

As discussed previously,[24] in comparison with the simulated curve obtained using the model that includes the T_1(H) effects, the simulated curve obtained by the pure spin diffusion model predicts a much lower magnetization recovery than experimentally observed. To fit the experimental data, a smaller domain size and relative larger interfacial thickness generally have to be used. Our interfacial thickness result for the amorphous SEO-1 sample obtained using a pure spin diffusion model further confirms this conclusion. Recently, De Paul et al.[35] have discussed the local chemical environments, dynamic heterogeneities, and nature of the interface in structured organic−inorganic composites prepared from poly(isoprene-*b*-ethylene oxide) block copolymers. They found that the separation of the polyisoprene from the poly(ethylene oxide) is expected to be sharp (less than 0.5 nm) because of the inherent incompatibility of these two polymers. In comparison with the interfacial thickness of less than 0.5 nm between the poly(isoprene) and poly(ethylene oxide) phases, a value of 1.5 nm interfacial thickness seems relatively larger than expected. This discrepancy is, at least partially, attributed to the usage of the pure spin diffusion model in the data analyses.[24]

Porod analysis of the SAXS synchrotron data at high q showed no evidence of the presence of a measurable interfacial thickness between the phases. However, a Porod plot of Iq^4 vs q^4 shows a clear positive deviation from the ideal zero slope case. This result can be attributed to the presence of electron density inhomo-

Table 5. Microdomain Structure Results from NMR and SAXS for SEO-1 Sample[a]

method	d_{PEO} (nm) (lamellae)	d_L (nm) (lamellae)	d_{PEO} (nm) (cylinder)	d_L (nm) (cylinder)	d_I (nm) (lamellae or cylinder)
NMR	8 ± 1	29 ± 3	14 ± 1	27 ± 3	1.5 ± 0.5
SAXS		42 ± 3		48 ± 3	

[a] d_L is the distance between the PEO domains, d_{PEO} is the diameter of the PEO domains for a cylinder system and is the length of the PEO domains for a lamellar system, and d_I is the interfacial thickness between the PS and the PEO domains.

geneities within the two phases occurring at length scales large relative to the molecular structure.[36] The possibility of incomplete phase separation may well obscure the effects of a finite but small interfacial region. No interfacial thickness can be obtained from the SAXS data for the SEO-1 sample.

3.3.2. Semicrystalline SEO Samples. Unlike the amorphous SEO-1, multiple scattering peaks at relative location of 1:2:3, in general, were found for semicrystalline SEO and PEO samples. This observation can be explained by the possible strong electron density contrasts between the amorphous PEO and crystalline PEO although no strong electron density contrast was found between the PS and the amorphous PEO phase. The relation of 1:2:3 for the peak locations is typical for a lamellar packed structure, and these results are generally consistent with previous studies by Gallot et al.[3−5] Recently, Sauer et al.[37] have studied poly(aryl ether ether ketone) and poly(ethylene terephthalate) semicrystalline materials and found that there are probably some pure amorphous regions outside of crystalline and amorphous layer structure. However, no glass transition temperatures are found for PS and PEO in all the SEO semicrystalline materials, indicating no pure amorphous regions, which tends to favor our model in which a lamellar layered structure is formed for the whole material. It should be acknowledged that there are some distortions related to the peak locations, and the competition between crystallization and regular phase separation is probably the main reason for these distortions. However, the 1:2:3 still works better than any other assumptions. It must be pointed out that orientation effects, in terms of a sheet texture, were observed in the original 2-dimensional scattering profile. This indicates the absence of completely global isotropic scattering from the crystalline phases. However, standard Lorentz corrections are still applicable in the absence of perfect orientation.[38]

The observed first-order maximum for all the samples can be explained as a result of interdomain distance between the lamellar layers and can be estimated by the following equation,

$$d_L(\text{SAXS}) = a = 2\pi/q_{max} \tag{6}$$

where a is the plane spacing associated with the first Bragg peak for a lamellar system and d_L is the interdomain distance which is equal to the plane spacing for a lamellar system. The calculated results for the semicrystalline SEO and PEO samples in Figure 2 are given in Table 6.

To obtain the interfacial structure information, SAXS Porod analysis was performed for all the samples. Porod analysis is generally performed in the region of the final slope of the scattered intensity. The simple geometric arguments that can be found in the texts by Glatter and Kratky[39] and Feigin and Svergun[36] lead to the prediction that the slope of the scattering goes as

Table 6. Microphase Structure Results from SAXS for Semicrystalline SEO and PEO Samples[a]

sample code	$q_{max} \pm 0.01$ nm^{-1}	d_L (nm) $\pm$ 3 nm	d_I (nm)
SEO-3	0.20	31	0.8 ± 0.3
SEO-4	0.24	26	2.1 ± 0.5
SEO-5	0.19	33	1.5 ± 0.4
PEO	0.33	19	2.1 ± 0.3

[a] d_L is the distance between the crystalline PEO domains, and d_I is the interfacial thickness between the crystalline PEO and amorphous PEO domains.

$$I = \frac{Q}{\pi}\frac{S}{V}\frac{1}{q^4} \tag{7}$$

The invariant, Q, is a measure of the total scattering intensity. The parameter S is the total interfacial area of the particle while the volume V would be the total volume occupied by the particle. That is, the specific surface, S/V, can be obtained from the final slope of the scattering curve given a valid estimate of the invariant, Q. Porod analysis is generally done by plotting the data in the form of Iq^4 vs q^4 and obtaining a value of the constant in the region of the final slope of the scattered intensity. This is, of course, the ideal case and very rarely seen in real materials. In real systems, there will be always be some heterogeneity within the phases due to atomic structure as well as possible phase intermixing. If the heterogeneity occurs at sufficiently small length scales, the resulting contribution may be represented as a constant in the small-angle region, and the corrected I_{corr} can be obtained by subtracting off the constant from the original data. The plot of $I_{corr}q^4$ vs q^4 will show a negative deviation from the ideal constant value at high q if a finite interfacial thickness between phases exists. Details about the use of Porod analysis to obtain interfacial thickness information can be found in the literature.[24,36]

Plots in the form of Iq^4 vs q^4 were made for all the semicrystalline SEO samples and the PEO sample, and a linear region of positive slope at high q was found in every case. In Figure 8, a typical plot of Iq^4 vs q^4 and a linear fitting at high q region for PEO are given. A corrected intensity is then obtained by subtracting the value of the slope of the linear fitting, and this scattering intensity was used for further analysis of the interfacial structure. Plots of $I_{corr}q^4$ vs q^4 were carried out for all the samples, and a negative deviation was found in all cases. Plots in the form of $\ln(I_{corr}q^4)$ vs q^2 for PEO and SEO-5 are given in Figures 9 and 10, respectively, and values of 2.1 and 1.5 nm interfacial thickness between the crystalline and amorphous PEO domain in PEO and SEO-5 samples were obtained assuming $d_I = (2\pi m)^{1/2}$, where $-m$ is the slope obtained from the linear fitting. In all cases, a region of negative slope, although very weak, is readily identified, and an interfacial thickness between the crystalline PEO and amorphous PEO is estimated to be about 2 nm for the majority of the

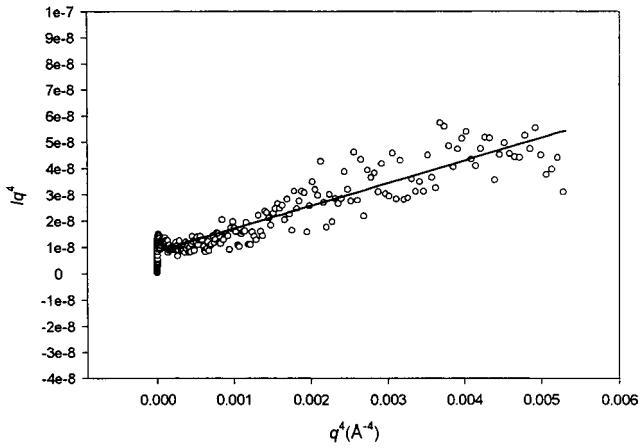

Figure 8. Porod plot in the form of Iq^4 as a function of q^4 for the PEO sample.

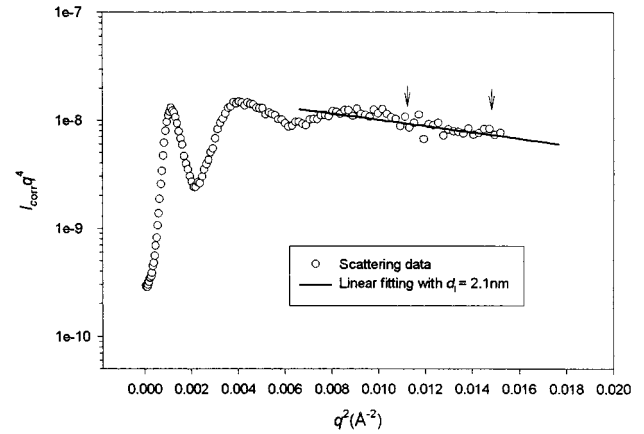

Figure 9. Porod plot after all background correction in the form of $\ln(I_{corr}q^4)$ as a function of q^2 for the PEO sample.

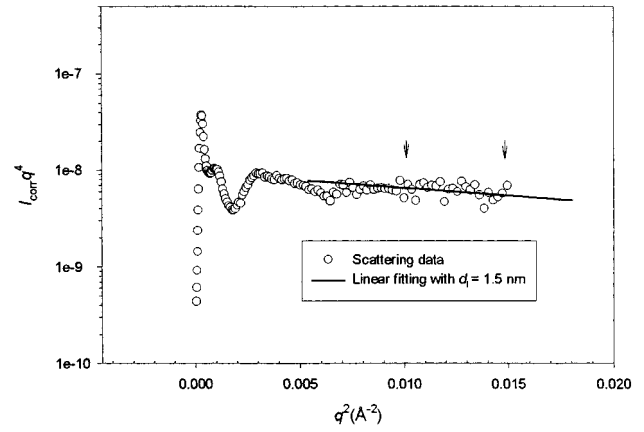

Figure 10. Porod plot after all background correction in the form of $\ln(I_{corr}q^4)$ as a function of q^2 for the SEO-5 sample.

semicrystalline SEO and PEO homopolymer, as given in Table 6.

4. Conclusions

The microphase structure of poly(styrene−ethylene oxide) block copolymers has been investigated by solid-state NMR and small-angle X-ray scattering techniques. Solid-state NMR of ^{1}H spin diffusion was used to determine the sizes of the PEO and the PS domains, interdomain distances, and the interfacial thickness between them using an initial-rate approximation and a pure spin diffusion model for the amorphous SEO-1 sample. It has been found that the domain sizes of the PEO domain and the interdomain distance obtained from the above two methods are generally in a good agreement, but the interdomain distance determined by the NMR method (27−29 nm) is relatively lower than the result (42−48 nm) obtained by SAXS. The discrepancy is probably due to the simulation model used in the NMR data interpretation. Although the simulation model including a T_1(H) term has been proven to be a more accurate model to extract the domain size parameters, the uncertainties associated with the intrinsic T_1-(H) values make this model unsuitable to systems where it is difficult to accurately determine this parameter; the pure spin diffusion model may be a good choice in this situation. An estimated 1.5 nm interfacial thickness between the PS and the amorphous PEO was found from the numerical simulation for the amorphous SEO-1 sample while SAXS analysis cannot provide this information for this sample. For the semicrystalline polymers, the relative locations of multiple scattering peaks and the locations of the first-order maximum in the SAXS scattering profiles were used to determine the morphology and interdomain distances of the materials. Porod analysis was used to estimate the interfacial thickness between the crystalline and amorphous PEO phases. It has been found that all the studied semicrystalline SEO samples have lamellar structures, and these results are generally consistent with the literature.[3−5] Solid-state NMR cannot provide this information on these semicrystalline block copolymer materials, and this is a typical example where the two techniques, NMR and SAXS, are complementary for the determination of the microphase structure of polymer materials.

Further analysis of the SAXS profiles, in combination with wide-angle X-ray scattering (WAXS) data can of course, be used to obtain even more structural information, such as crystallinity, crystal structure, and the thickness of the PEO crystalline layer. This work is in progress.

Acknowledgment. We thank the Natural Science and Engineering Research Council (NSERC) of Canada and the Environmental Science and Technology Alliance of Canada (ESTAC) for their financial support. We also thank the Laboratorio Nacional de Luz Síncrotron (LNLS) in Brazil for assistance with the synchrotron SAXS measurements.

References and Notes

(1) Noshay, A.; McGrath, J. E. In *Block Copolymers: Overview and Critical Survey*; Academic Press: New York, 1977; Chapter 3.
(2) Helfand, E.; Wasserman, Z. R. In *Development in Block Copolymers*; Goodman, J., Ed.; Applied Science: New York, 1982; Vol. 1.
(3) Gallot, B. *Adv. Polym. Sci.* **1978**, *29*, 85.
(4) Gervais, M.; Gallot, B. *Polymer* **1981**, *22*, 1124.
(5) Gervais, M.; Gallot, B. *Makromol. Chem.* **1973**, *171*, 157; **1973**, *174*, 193; **1977**, *178*, 1577; **1977**, *178*, 2071; **1979**, *180*, 2041.
(6) DiMarzio, E. A.; Guttman, C. M.; Hoffman, J. D. *Macromolecules* **1980**, *13*, 1194.
(7) Floudas, G.; Tsitsilianis, C. *Macromolecules* **1997**, *30*, 4381.
(8) VanderHart, D. L.; Manley, R. S. J.; Barnes, J. D. *Macromolecules* **1994**, *27*, 2826.
(9) Jack, K. S.; Natansohn, A.; Wang, J.; Favis, B. D.; Cigana, P. *Chem. Mater.* **1998**, *10*, 1031.
(10) White, J. L.; Brant, P. *Macromolecules* **1998**, *31*, 5424.
(11) Schmidt-Rohr, K.; Clauss, J.; Blümich, B.; Spiess, H. W. *Magn. Reson. Chem.* **1990**, *28*, S3.

(12) Cai, W. Z.; Schmidt-Rohr, K.; Egger, N.; Gerharz, B.; Spiess, H. W. *Polymer* **1993**, *34*, 267.
(13) Cho, G.; Natansohn, A.; Ho, T.; Wynne, K. J. *Macromolecules* **1996**, *29*, 2563.
(14) Schmidt-Rohr, K.; Spiess, H. W. In *Multidimensional Solid State NMR and Polymers*; Academic Press: London, 1994.
(15) Jack, K. S.; Wang, J.; Natansohn, A.; Register, R. A. *Macromolecules* **1998**, *31*, 3282.
(16) Havens, J. R.; VanderHart, D. L. *Macromolecules* **1985**, *18*, 1663.
(17) Kimura, T.; Neki, K.; Tamura, N.; Horii, F.; Nakagawa, M.; Odani, H. *Polymer* **1992**, *33*, 493.
(18) Eckman, R. R.; Henrichs, P. M.; Peacock, A. J. *Macromolecules* **1997**, *30*, 2474.
(19) Clayden, N. *J. Polym. Sci., Part B: Polym. Phys.* **1994**, *32*, 2321.
(20) Clauss, J.; Schmidt-Rohr, K.; Spiess, H. W. *Acta Polym.* **1993**, *44*, 1.
(21) Wang, J.; Jack, K. S.; Natansohn, A. *J. Chem. Phys.* **1997**, *107*, 1016.
(22) Wang, J. *J. Chem. Phys.* **1996**, *104*, 4850.
(23) Yu, H.; Wang, J.; Natansohn, A.; Singh, M. A. *Macromolecules* **1999**, *32*, 4365.
(24) Yu, H.; Natansohn, A.; Singh, M. A.; Plivelíc, T. *Macromolecules* **1999**, *32*, 7562.
(25) Richardson, M. J.; Savill, N. G. *Polymer* **1977**, *18*, 3.
(26) Miller, R. L.; Lee, W. A.; Rutherford, R. A. In *Polymer Handbook*, 2nd ed.; Brandrup, J., Immergut, E. H., Eds.; Wiley-Interscience: New York, 1975; Vol. III.
(27) Egger, N.; Schmidt-Rohr, K.; Blümich, B.; Dmmke, W. D.; Stapp, B. *J. Appl. Polym. Sci.* **1992**, *44*, 289.
(28) Kellermann, G.; Vicentin, F.; Tamura, E.; Rocha, M.; Tolentino, H.; Barbosa, A.; Craievich, A.; Torriani, I. *J. Appl. Crystallogr.* **1997**, *30*, 880.
(29) Demco, D. E.; Johansson, A.; Tegenfeldt, J. *Solid State Nucl. Magn. Reson.* **1995**, *4*, 13.
(30) Wilhelm, M.; Lehmann, S.; Jäger, C.; Spiess, H. W. *Magn. Reson. Chem.* **1994**, *32*, S3.
(31) Spiegel, S.; Schmidt-Rohr, K.; Boeffel, C.; Spiess, H. W. *Polymer* **1993**, *34*, 4566.
(32) Mellinger, F.; Wilhelm, M.; Spiess, H. W. *Macromolecules* **1999**, *32*, 4686.
(33) Van Den Bossche, G.; Sobry, R.; Frédéric, F.; Clacens, J.-M.; Gabelica, Z. *J. Appl. Crystallogr.* **1997**, *30*, 1065
(34) Sakurai, S.; Kawada, H.; Hashimoto, T. *Macromolecules* **1993**, *26*, 5796.
(35) De Paul, S. M.; Zwanziger, J. W.; Ulrich, R.; Wiesner, U.; Spiess, H. W. *J. Am. Chem. Soc.* **1999**, *121*, 5727.
(36) Feigin, L. A.; Svergun, D. I. In *Structure Analysis by Small-Angle X-ray and Neutron Scattering*; Plenum Press: New York, 1987.
(37) Sauer, B. B.; Hsiao, B. S. *Polymer* **1995**, *36*, 2553.
(38) Sakurai, S.; Okamoto, S.; Kawamura, T.; Hashimoto, T. *J. Appl. Crystallogr.* **1991**, *24*, 679.
(39) Glatter, O.; Kratky, O. In *Small-Angle X-ray Scattering*; Academic Press: London, 1982.

MA001127B